

Modeling of traveling-wave amplification photodetectors (TAP detectors)

Daniel Lasasoa, Yi-Jen Chiu, Joachim Piprek, and John E. Bowers

Department of Electrical and Computer Engineering,

University of California at Santa Barbara, Santa Barbara, CA 93106

ABSTRACT

High speed, high efficiency, low noise and high saturation power are the characteristics desired for detectors in high bit-rate long-haul optical communication systems. We present the modeling of Traveling-wave Amplification Photodetectors (TAP detectors). These novel monolithic devices combine optical gain and absorption in a distributed fashion along a traveling-wave structure, providing high-responsivity and high-speed performance, without sacrificing saturation power. We present the models used to simulate the behavior of these devices, as well as their results. We show that TAP detectors have higher saturation power than other detectors with the same bandwidth-efficiency product, at the price of a small noise penalty, which is also calculated. The result is a net increase in the dynamic range.

Keywords: photodetector, traveling-wave, optical gain, distributed gain, distributed detection, bandwidth-efficiency product, saturation power, slow-wave effects, noise, dynamic range.

1. INTRODUCTION

Vertically illuminated photodetectors present bandwidth-efficiency limitations. Traveling-Wave Photodetectors (TWPDs) can overcome those [1]. In order to increase the photocurrent without the use of an Erbium-Doped Fiber Amplifier (EDFA), a Semiconductor Optical Amplifier (SOA) can be integrated with a TWPD, in order to obtain high efficiency and bandwidth [2]. This comes at the price of relatively low saturation power because of field-screening effects in the photodetector, due to the high optical powers present in the device. Velocity-Matched Photodetectors (VMPDs) allow for high saturation power, and eliminate the frequency limitation due to walk-off between electrical and optical waves propagating along the device [3], at the price of lower efficiency. In order to combine high saturation power, high speed and high efficiency, Traveling-wave Amplification Photodetectors have been studied [4]. These devices combine optical gain and absorption in a single waveguide in a distributed way.

TAP detectors with a parallel configuration feature a single waveguide with three longitudinal contacts separated laterally, as shown in Fig. 1.a. The one in the center is forward-biased in order to provide gain, and the two on the sides reverse-biased for detection. This configuration features optimum overlap between the peak of the mode and the optical gain, as well as low confinement factor for the absorption region, thus avoiding field-screening effects. The result is a higher saturation power. When gain, absorption and losses per unit length cancel out exactly, the optical power present in the waveguide is constant along the device length, making it possible to have arbitrarily long devices, consequently featuring arbitrarily high efficiency.

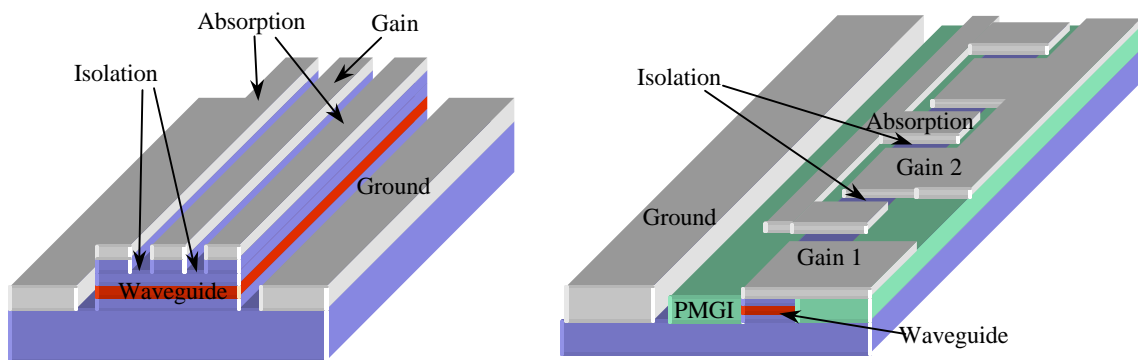


Fig. 1: TAP detector configurations: a) parallel (left), b) sequential (right).

In terms of microwave propagation, parallel TAP detectors can be simulated by a ground-signal-ground-signal-ground line (GSGSG line), the central conductor being DC forward-biased, but not carrying any AC signal. Slow-wave effects need to be taken into account due to the presence of doped layers underneath the two DC reverse-biased signal lines. Velocity and impedance mismatch effects are important, and will limit the overall device performance.

TAP detectors with a sequential configuration present an optical waveguide with longitudinally alternating periods of optical gain and absorption, as shown in Fig. 1.b. The input optical signal is amplified and partially absorbed several times providing, for the same saturation power, higher gain than traditional detectors with optical preamplification, as shown in Fig. 2. The first gain section may be longer and separately biased for higher amplification. When the gain, absorption and losses in each period cancel out exactly, the optical power that will arrive to each detection section is constant, making it possible to have devices with many periods, and thus very high efficiency.

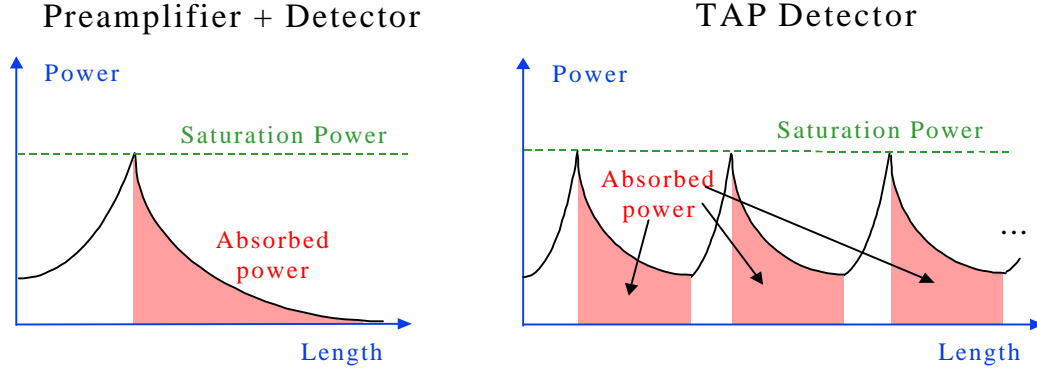


Fig. 2: Comparison of efficiency in sequential TAP detectors and traditional photodetectors with preamplification for the same saturation power.

In terms of microwave propagation, sequential TAP detectors behave as a periodically loaded grounded Coplanar Waveguide (CPW), since the DC forward-biased gain electrode carries no signal. Velocity and impedance matching for these devices is possible by adequately choosing the ratio between gain and absorption lengths in each period. These characteristics make it possible for detectors with many periods to present high bandwidths. The device performance will be limited mostly by microwave losses.

Since optical amplification is introduced, noise becomes an important issue in these devices. Furthermore, due to the distributed nature of both configurations, traditional models are not adequate for noise simulations. Therefore, a distributed noise model was developed and used in both configurations, showing that the higher saturation power of TAP detectors provides a net increase in the dynamic range with respect to photodetectors with similar bandwidth-efficiency product.

2. MICROWAVE MODEL

Coplanar Waveguides (CPWs) are one of the most usual structures for microwave transmission in fast optoelectronic devices, due to good high frequency characteristics and easy access for interconnects. It is well known that the presence of doped semiconductor layers under the signal line in a CPW produces slow-wave effects [5], which result in lower propagation speed and higher electrical losses. Any high-frequency (>1GHz) model of traveling-wave semiconductor optoelectronic devices must take these into account. Excess losses due to skin effect in the conductor must also be included in the calculation. Distributed element models taking into account all these effects have been used in the past to study the performance of traditional Traveling-Wave Photodetectors (TWPDs) [6]. TAP detectors may be simulated also using these models, but modifications need to be made in order to properly describe their particular geometries.

2.1. Parallel configuration

2.1.1. Distributed element model

In the case of parallel TAP detectors, the electrical waveguide presents a GSGSG configuration, where the central electrode, being DC forward biased, doesn't carry any signal. We need then to change the model to take into account the double signal line. Furthermore, an extra component needs to be introduced in the parallel admittance, to describe the effect of the semiconductor connecting each signal line to the central ground conductor, as shown in Fig. 3. The terms describing the series inductance and parallel capacitance associated purely to the conductor geometry need to be those of a GSGSG line,

instead of those of a pure GSG line. These were simulated using the commercially available package Momentum from Agilent. The S-parameters of such a structure were found first, and then its microwave propagation characteristics were calculated, using the relation (see for example [7]):

$$\begin{bmatrix} \cosh(\mathbf{g} \cdot L) & Z \cdot \sinh(\mathbf{g} \cdot L) \\ \frac{\sinh(\mathbf{g} \cdot L)}{Z} & \cosh(\mathbf{g} \cdot L) \end{bmatrix} = \begin{bmatrix} \frac{(1+S_{11}) \cdot (1-S_{22}) + S_{12} \cdot S_{21}}{2 \cdot S_{21}} & Z_0 \cdot \frac{(1+S_{11}) \cdot (1+S_{22}) - S_{12} \cdot S_{21}}{2 \cdot S_{21}} \\ \frac{1}{Z_0} \cdot \frac{(1-S_{11}) \cdot (1-S_{22}) - S_{12} \cdot S_{21}}{2 \cdot S_{21}} & \frac{(1-S_{11}) \cdot (1+S_{22}) + S_{12} \cdot S_{21}}{2 \cdot S_{21}} \end{bmatrix}; \quad (1)$$

where $\mathbf{g} = \mathbf{a} + j \cdot \mathbf{b}$ is the microwave propagation constant and Z the characteristic impedance of the line, and $Z_0 = 50\Omega$ the reference impedance at both sides of said line. Finally, the values of inductance L and capacitance C were fitted to the result, by the use of the well known relations (see for example [8]):

$$\operatorname{Re}[Z^2] = \frac{\frac{L}{C} \cdot \omega^2 + \frac{R \cdot G}{C^2}}{\omega^2 + \frac{G^2}{C^2}}, \quad \left| \frac{d^2(\mathbf{g}^2)}{d\omega^2} \right| = L \cdot C. \quad (2)$$

The rest of the elements in the model, such as the metal impedance Z_m , the longitudinal and transverse impedances associated to the semiconductor epilayers, Z_l and Z_t , respectively, the capacitance of the intrinsic region C_i , and the impedance associated to the substrate, Z_{sb} , are calculated as always (see, for example, [9])

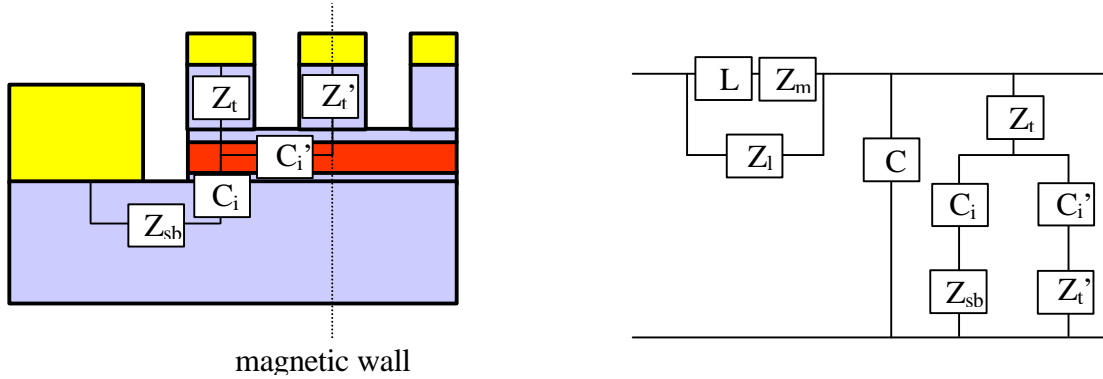


Fig. 3: Left: diagram showing the origin of the extra terms in the parallel admittance. Right: distributed element model for parallel TAP detectors

2.1.2. Simulation results

Fig 4.a shows the simulation results for parallel TAP detectors when this model was used. We can see that, according to what could be expected, slow-wave effects produce an effective propagation index quite higher than the optical one ($n_{par} \sim 10$), a low characteristic impedance ($Z_{par} \sim 20\Omega$) and a relatively high loss α_{par} increasing with frequency, its value being $\sim 40\text{cm}^{-1}$ at 100GHz. In such a device, we can predict that the microwave bandwidth will be loss-limited.

Parallel TAP detectors were fabricated and their S-parameters measured. From them, using again equation (1), their characteristic impedance and microwave propagation coefficient were calculated. Fig 4.b shows the comparison between the experimental results and the theoretical prediction found using the model. The good agreement validates the model that has been developed to simulate these devices.

2.2. Sequential configuration

2.2.1 ABCD matrix

Sequential TAP detectors present a periodic structure; in their absorption sections, slow-wave effects are present. We need to find a calculation method that allows us to find, for such configuration, the microwave propagation parameters. We chose to use the ABCD matrix, since its characteristics are appropriate for this situation. For an ABCD matrix calculation to be valid in a periodic structure, the period length needs to be much shorter than the guided electrical wavelength; otherwise the presence of resonances makes the results incorrect. For a frequency of 300GHz, the free space

wavelength associated is $\sim 1\text{mm}$. Therefore, choosing a period of $50\mu\text{m}$, 20 times smaller, the ABCD calculation results will be valid at least up to that frequency. In order to be able to obtain reasonable electrical isolation between the gain and absorption contacts, we choose the separation between them to be $2\mu\text{m}$. Keeping then these two lengths constant, different simulations will be performed for different values of the absorption section length.

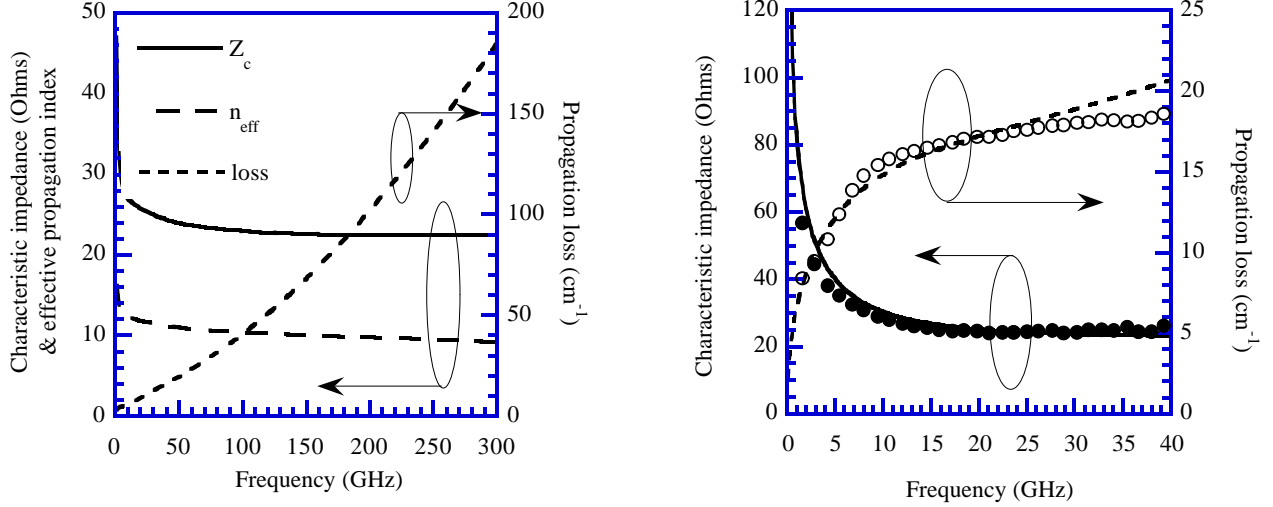


Fig. 4: a) Left: Simulated microwave propagation characteristics for parallel TAP detectors. b) Right: Comparison between theoretical (line) and experimental (symbol) values for characteristic impedance and microwave loss.

In order to set up a simulation using the ABCD matrix, we remember that the relation between itself and the microwave propagation parameters is (see for example [9]):

$$\begin{bmatrix} A & B \\ C & D \end{bmatrix} = \begin{bmatrix} \cosh(\mathbf{g} \cdot L) & Z \cdot \sinh(\mathbf{g} \cdot L) \\ \frac{\sinh(\mathbf{g} \cdot L)}{Z} & \cosh(\mathbf{g} \cdot L) \end{bmatrix}. \quad (3)$$

We can therefore find the ABCD matrix parameters for the different sections of the device, knowing their length, characteristic impedance and microwave propagation constant, and multiply them in order to find the ABCD matrix of a period, as given by:

$$\begin{bmatrix} A & B \\ C & D \end{bmatrix}_{\text{period}} = \begin{bmatrix} A & B \\ C & D \end{bmatrix}_{\text{gain}} \cdot \begin{bmatrix} A & B \\ C & D \end{bmatrix}_{\text{isolation}} \cdot \begin{bmatrix} A & B \\ C & D \end{bmatrix}_{\text{absorption}} \cdot \begin{bmatrix} A & B \\ C & D \end{bmatrix}_{\text{isolation}}. \quad (4)$$

From the ABCD matrix parameters for the period, we can calculate the microwave propagation constant and impedance associated to it, which are the same for the entire detector. The ABCD matrix parameters for each section were calculated using a similar distributed element model as was used for parallel TAP detectors, dropping all semiconductor related terms in the gain and absorption regions, since the signal electrode travels on top of an insulator.

2.2.2 Simulation results

Simulations were performed using values for the absorption section length of 4, 6 and $8\mu\text{m}$. The optical waveguide and the top contact ridge are assumed to be 6 and $3\mu\text{m}$ wide, respectively. The results, shown in Fig. 5, agree with our intuitive prediction of behavior close to impedance and velocity matching. We can also see that the microwave losses are small ($<10\text{cm}^{-1}$) up to 100GHz, which makes long devices with many periods possible. Finally, we can also observe that, for increasing absorption section length, the capacitive loading to the electrical waveguide also increases, as well as the importance of slow-wave effects, resulting in higher losses, and lower impedance and propagation velocity.

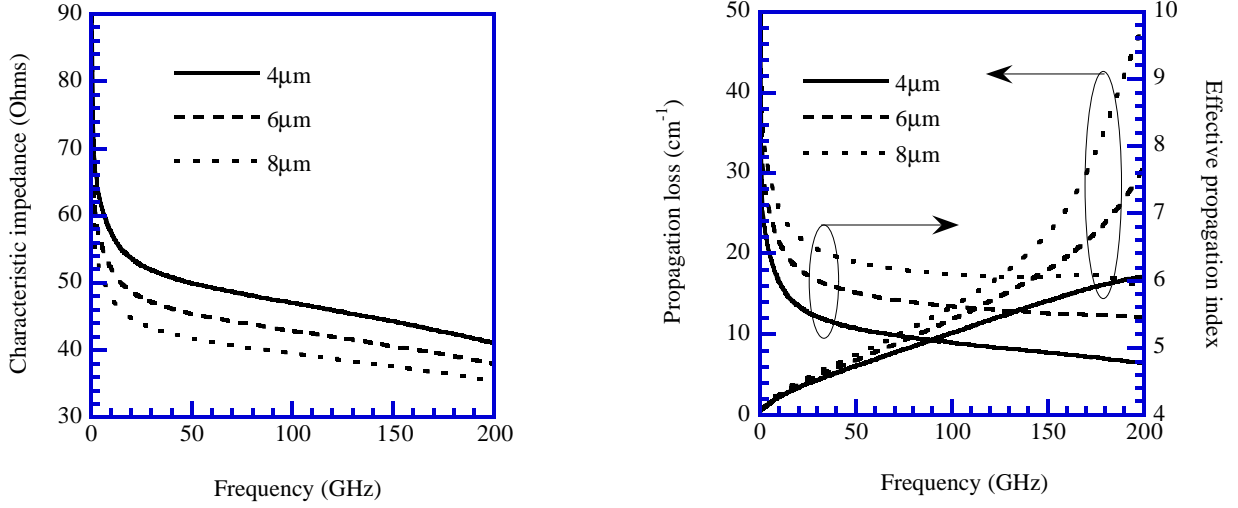


Fig. 5: Simulated microwave characteristics of sequential TAP detectors for different absorption section lengths. Left: Characteristic impedance. Right: Propagation index and loss. Period and isolation region are 50 and $2\mu\text{m}$.

3. ELECTRO-OPTIC RESPONSE

3.1. Parallel configuration

In order to find the electro-optic response of parallel TAP detectors, a distributed photocurrent model is used. The device is divided up in sections of length dz . In each one of them, the position-dependent optical power will be found. From it, a local photocurrent source can be calculated. This photocurrent will be propagated using the microwave characteristics that we already found, and added for the total length of the detector in order to find the total response.

3.1.1. Position-dependent current source

Let P_{opt} be the input optical power, and \mathbf{h}_c the coupling efficiency. When gain, absorption and losses cancel out exactly, the optical power in the device is constant with length. However, we need to allow for mismatch between these three quantities. We can therefore define a net modal gain per unit length Δg for the device as:

$$\Delta g = \Gamma_g \cdot g - \Gamma_{abs} \cdot \mathbf{a}_{opt} - \mathbf{a}_L, \quad (5)$$

where Γ_g and Γ_{abs} are the gain and absorption confinement factors, respectively, g is the material gain per unit length, \mathbf{a}_{opt} is the material optical absorption and \mathbf{a}_L are the modal losses, due to effects such as scattering and free-carrier absorption.

In each element of length dz , a position-dependent photocurrent dI_{ph} is generated, its value being:

$$dI_{ph}(\mathbf{w}, z) = \frac{e \cdot \mathbf{h}_c \cdot P_{opt}}{\hbar \mathbf{w}} \cdot \frac{1}{1 + j \cdot \mathbf{w} \cdot t_{eff}} \cdot e^{\left(\Delta g - j \cdot \frac{\mathbf{w} \cdot n_o}{c}\right) z} \cdot \Gamma_{abs} \cdot \mathbf{a}_{opt} \cdot dz, \quad (6)$$

where the optical propagation index n_o is introduced in order to take into account the walk-off between electrical and optical waves propagating along the device, and t_{eff} models the frequency response of the active region, where

$$\frac{1}{t_{eff}} = \frac{1}{t_{life}} + \frac{1}{t_{transit}}, \quad (7)$$

t_{life} being the carrier lifetime in the active region, and $t_{transit}$ the carrier transit time across it.

3.1.2. Distributed photocurrent model

Once the generated photocurrent in each section has been found out, we need to simulate its propagation up to the end of the device, using the microwave propagation characteristics that we have calculated. The forward and backward propagating currents, I_{fwd} and I_{bck} , can be expressed as:

$$\begin{aligned}
I_{fwd}(\mathbf{w}) &= \frac{1}{2} \cdot \int_0^L dI_{ph}(\mathbf{w}, z) \cdot e^{-\mathbf{g}_{par}(\mathbf{w}) \cdot (L-z)}, \\
I_{bck}(\mathbf{w}) &= \frac{1}{2} \cdot \int_0^L dI_{ph}(\mathbf{w}, z) \cdot e^{-\mathbf{g}_{par}(\mathbf{w}) \cdot (L+z)}.
\end{aligned} \tag{8}$$

The effect of impedance mismatch is taken into account by writing the total photocurrent as:

$$I_{par}(\mathbf{w}) = \frac{1 - \Gamma(\mathbf{w})}{1 - \Gamma(\mathbf{w}) \cdot e^{-j \cdot 2 \cdot \mathbf{g}_{par} \cdot L}} \cdot (I_{fwd}(\mathbf{w}) + I_{bck}(\mathbf{w})), \tag{9}$$

where the frequency-dependent reflection coefficient between the device and the load of impedance Z_L , Γ , is defined, as always, by (see for example [9]):

$$\Gamma(\mathbf{w}) = \frac{Z_L - Z_{car}(\mathbf{w})}{Z_L + Z_{car}(\mathbf{w})}. \tag{10}$$

The results of the previous calculation yield:

$$\begin{aligned}
|I_{par}(\mathbf{w})| &= \frac{e \cdot \mathbf{h}_c \cdot P_{opt} \cdot \Gamma_{abs} \cdot \mathbf{a}_{opt}}{2 \cdot \hbar \mathbf{w}} \cdot \left| \frac{1}{1 + j \cdot \mathbf{w} \cdot t_{eff}} \right| \cdot \left| \frac{1 - \Gamma(\mathbf{w})}{1 - \Gamma(\mathbf{w}) \cdot e^{-j \cdot 2 \cdot \mathbf{g}_{par} \cdot L}} \right| \cdot \\
&\quad \left| \frac{e^{\Delta g \cdot L} - e^{-\left(\mathbf{a}_{par} + j \cdot \frac{\mathbf{w}(n_{par} - n_o)}{c}\right) \cdot L}}{\Delta g + \mathbf{a}_{par} + j \cdot \frac{\mathbf{w} \cdot (n_{par} - n_o)}{c}} + \frac{e^{\left(\Delta g - 2\mathbf{a}_{par} - j \cdot \frac{2\mathbf{w} \cdot n_{par}}{c}\right) \cdot L} - e^{-\left(\mathbf{a}_{par} + j \cdot \frac{\mathbf{w}(n_{par} - n_o)}{c}\right) \cdot L}}{\Delta g - \mathbf{a}_{par} - j \cdot \frac{\mathbf{w} \cdot (n_{par} + n_o)}{c}} \right|,
\end{aligned} \tag{11}$$

which we can use to plot the total frequency-dependent photocurrent in order to find the device bandwidth.

Defining the efficiency \mathbf{h}_{par} as the number of photocurrent electrons generated per optical input photon in a parallel TAP detector, we find that the DC efficiency is:

$$\mathbf{h}_{par} = \frac{|I_{par}(0)|}{\frac{e}{\hbar \mathbf{w}}} = \mathbf{h}_c \cdot \Gamma_{abs} \cdot \mathbf{a}_{opt} \cdot \frac{e^{\Delta g \cdot L} - 1}{\Delta g} \approx \mathbf{h}_c \cdot \Gamma_{abs} \cdot \mathbf{a}_{opt} \cdot L, \tag{12}$$

where the last approximation is valid when $\Delta g \cdot L \ll 1$, i.e., when the net modal gain is very small and the optical power along the detector can be considered constant. Under this condition, as could be expected, the efficiency is directly proportional to the device length.

3.1.3. Bandwidth-efficiency product

Combining the microwave characteristics shown in Fig. 4 with equations (11) and (12), we find the efficiency and bandwidth. Fig. 6 shows that the bandwidth is roughly inversely proportional to the device length, and otherwise limited by the active region response; it does not depend on the net modal gain Δg . Also, when $\Delta g = 0$, the efficiency is proportional to the device length, and becomes greater than 1 for device lengths higher than 150 μm .

For $\Delta g = 0$, this results in a constant bandwidth-efficiency product of ~80GHz for device lengths higher than 150 μm . Now, this value is similar to that of traditional TWPDs [1], with the added advantage in this case that, the absorption confinement factor being about 20 times smaller, the optical power needed to saturate the device due to field-screening effects is 13dB higher. For short devices, the bandwidth-efficiency product is lower because the bandwidth is not limited by microwave loss, but by the active region response time.

When $\Delta g > 0$, higher values of efficiency are possible, the price being a lower saturation power, due to the increase of the optical field from its initial valued as the wave propagates along the device.

When $\Delta g < 0$, saturation will occur only if the optical power is high enough close to the input, but efficiency will be lower in this case. The full potential of the device is not optimally taken advantage of, and we can conclude that best operation condition is for the net modal gain to be either zero or positive and small ($\sim 20\text{cm}^{-1}$), depending on whether the main goal is higher saturation power or higher efficiency. The net modal gain can be adjusted by changing only the bias current of the gain region; this degree of freedom allows for customized, or even adaptative device performance.

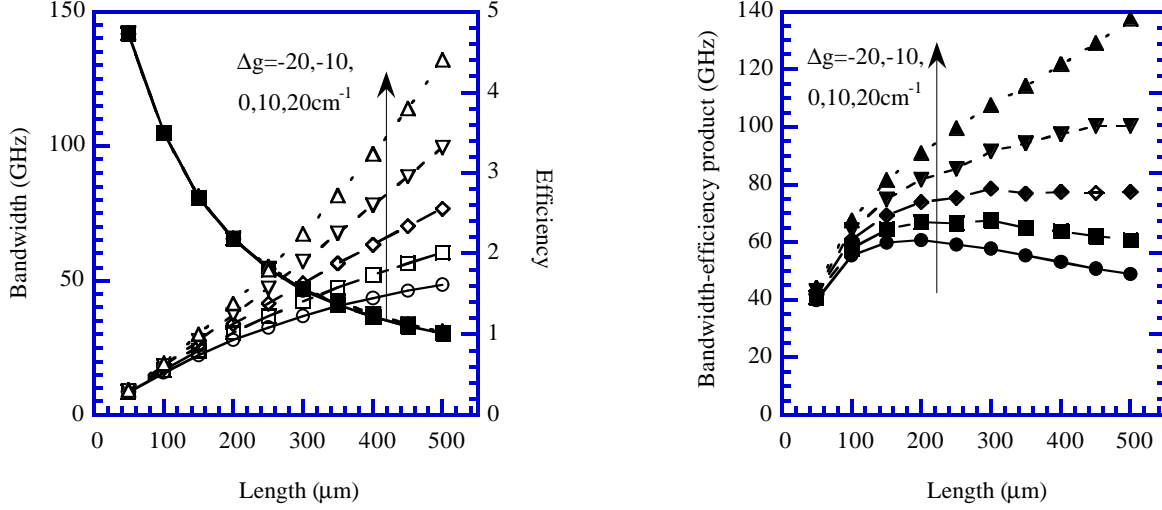


Fig. 6: Efficiency, bandwidth (left) and bandwidth-efficiency product vs. length for TAP detectors with different net modal gain.

3.2. Sequential configuration

Each detection section in the sequential configuration can be assimilated to a short TWPD. Each one of them will then be treated as an individual detector, whose response will be calculated. The different photocurrents will then be propagated using the microwave propagation characteristics that we found, and added up to find the total response.

3.2.1. Current source in each section

We can define a net gain per period ΔG in the sequential configuration, as the ratio between the optical power that arrives to consecutive detection regions, to take into account a possible mismatch between gain, absorption and losses in each period. It can be calculated to be:

$$\Delta G = G_2 \cdot (1 - \mathbf{h}_{det}) \cdot e^{-\mathbf{a}_L \cdot L_{per}}, \quad (13)$$

where G_2 is the gain in the amplification section of each period, \mathbf{h}_{det} is the fraction of photons absorbed in each detection section, and \mathbf{a}_L are the average optical losses per unit length, including effects such as absorption in the isolation regions, scattering and free carrier absorption. Defining G_1 as the gain in the first amplification section (which can be longer and independently biased for higher total efficiency), we find that the amount of optical power to arrive to the n -th detector is:

$$P_n = \mathbf{h}_c \cdot G_1 \cdot P_{opt} \cdot \Delta G^{n-1}. \quad (14)$$

The same distributed element model that can be used to calculate the ABCD matrix of the absorption section and the characteristics of each individual detector. Since we assume that the device is terminated in both ends, the only photocurrent component that interests us from each detector is just the forward propagating one. Then, knowing the microwave propagation characteristics for each individual detector, \mathbf{a}_{det} and n_{det} , the current generated from the n -th detector can be expressed as:

$$I_n(\mathbf{w}) = \frac{1}{2} \cdot \frac{1}{1 + j \cdot \mathbf{w} \cdot t_{eff}} \cdot \int_0^{L_{det}} \frac{e \cdot P_n}{\hbar \mathbf{w}} \cdot e^{-\left(\Gamma_{abs} \cdot \mathbf{a}_{opt} + j \cdot \frac{\mathbf{w} \cdot n_o}{c}\right) z} \cdot \Gamma_{abs} \cdot \mathbf{a}_{opt} \cdot dz \cdot e^{-\mathbf{g}_{det}(\mathbf{w}) \cdot (L_{det} - z)}. \quad (15)$$

3.2.2. Total photocurrent

The photocurrents from all individual sections must be added taking into account the velocity mismatch between them, as well as the microwave attenuation along the device, as expressed in the following equation:

$$I_{seq}(\mathbf{w}) = \sum_{n=1}^N I_n(\mathbf{w}) \cdot e^{-\left(\mathbf{a}_{seq} + j \cdot \frac{\mathbf{w}(n_{seq} - n_o)}{c}\right) \cdot (N-n) \cdot L_{per}}, \quad (16)$$

where N is the total number of periods, leading to the final result:

$$|I_{seq}(\mathbf{w})| = \frac{e \cdot \hbar c \cdot G_1 \cdot P_{opt} \cdot \Gamma_{abs} \cdot \mathbf{a}_{opt}}{2 \cdot \hbar \mathbf{w}} \cdot \left| \frac{1}{1 + j \cdot \mathbf{w} \cdot t_{eff}} \right| \cdot \left| \frac{e^{-\mathbf{a}_{det} \cdot L_{det}} - e^{-\left(-\Gamma_{abs} \cdot \mathbf{a}_{opt} + j \cdot \frac{\mathbf{w}(n_{det} - n_o)}{c}\right) \cdot L_{det}}}{\Gamma_{abs} \cdot \mathbf{a}_{opt} - \mathbf{a}_{det} - j \cdot \frac{\mathbf{w} \cdot (n_{det} - n_o)}{c}} \right| \cdot \left| \frac{\Delta G^N - e^{-\left(\mathbf{a}_{seq} + j \cdot \frac{\mathbf{w}(n_{seq} - n_o)}{c}\right) \cdot N \cdot L_{per}}}{\Delta G - e^{-\left(\mathbf{a}_{seq} + j \cdot \frac{\mathbf{w}(n_{seq} - n_o)}{c}\right) \cdot L_{per}}} \right|. \quad (17)$$

We can also calculate the DC efficiency, again in number of electrons of photocurrent per number of photons of optical input, as:

$$h_{seq} = \frac{\frac{|I_{seq}(0)|}{e}}{\frac{P_{opt}}{\hbar \mathbf{w}}} = \frac{\hbar c \cdot G_1 \cdot (1 - e^{-\Gamma_{abs} \cdot \mathbf{a}_{opt} \cdot L_{det}})}{2} \cdot \frac{\Delta G^N - 1}{\Delta G - 1} \approx \frac{\hbar c \cdot G_1 \cdot N \cdot (1 - e^{-\Gamma_{abs} \cdot \mathbf{a}_{opt} \cdot L_{det}})}{2}, \quad (18)$$

where the last approximation is valid when $\Delta G^N \approx 1$, i.e., when the optical power in the last section is not significantly different from the optical power in the first one. As expected, in that case the total efficiency is just proportional to the number of sections in the device.

3.2.3. Bandwidth-efficiency product

Fig. 7 shows the calculated bandwidth and bandwidth-efficiency product for sequential TAP detectors with different absorption section lengths, for a total optical gain of 20 in the first amplification section. The most interesting feature is that the bandwidth-efficiency product does not increase with the number of periods after 10, where the bandwidth is still in the 50-100GHz range. Therefore, it is possible to have high-speed sequential TAP detectors with gain-bandwidth products close to 2THz, with an optical gain 5 times lower than the one needed when TWPDS preceded by one single optical amplifier are used [2]. This translates into an increase of 7dB in the saturation power for the same response.

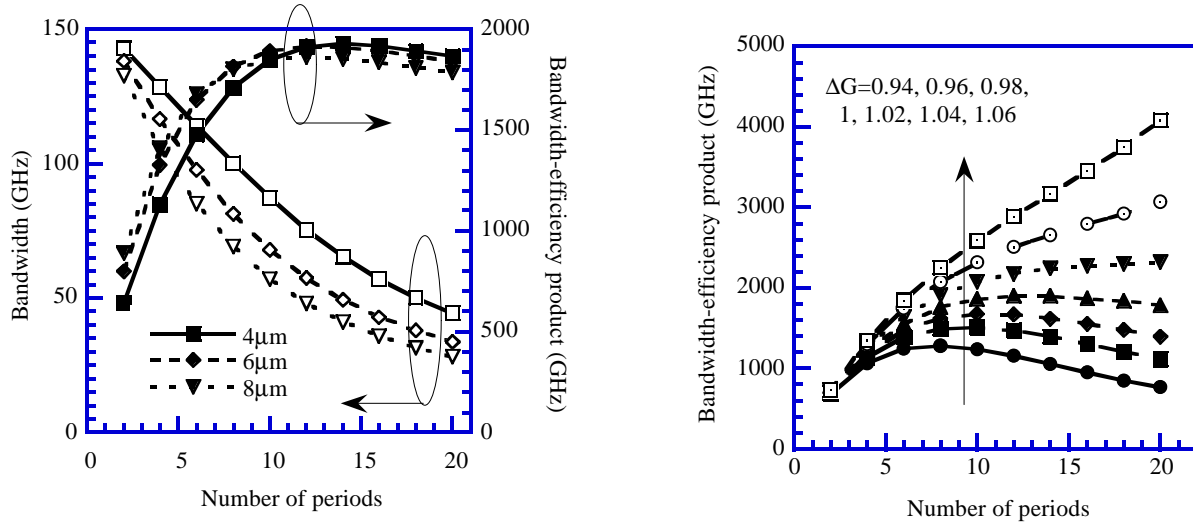


Fig. 7: Left: Bandwidth (empty symbols) and bandwidth-efficiency product (full symbols) vs. number of periods for sequential TAP detectors with different absorption section lengths, the net gain per period being 1. Right: Effect of net gain per period in the efficiency bandwidth product for an absorption section length of 4μm.

Fig. 7 also shows the effect of changes in the net gain per period on the detector response. We can see that bandwidth-efficiency product increases rapidly with ΔG , for a twofold reason: first, the efficiency obviously increases, and second, the bandwidth does two, since the sections of the device near its end, whose photocurrent is going to suffer less

microwave loss, are absorbing more optical power. Now, for 20 periods and $\Delta G = 1.06$, the optical power in the last absorption section is still less than 5 times larger than in the first one, while the bandwidth-efficiency product has raised up to ~ 4 THz. Therefore, for the same saturation power, sequential TAP detectors can have much higher bandwidth-efficiency products than TAPDs with preamplification.

4. NOISE

Current noise in photodetectors is given by:

$$\langle i_N^2 \rangle = \left(\frac{4 \cdot k_B T}{R_L} + 2 \cdot e \cdot I_d + \mathbf{s}_{sg}^2 + \mathbf{s}_{sp}^2 + \mathbf{s}_{sg-sp}^2 + \mathbf{s}_{sp-sp}^2 \right) \cdot \Delta f, \quad (19)$$

where Δf is the device bandwidth, R_L is the load resistance, I_d is the dark current, \mathbf{s}_{sg}^2 and \mathbf{s}_{sp}^2 are the shot noise terms associated to the signal and spontaneous emission, and \mathbf{s}_{sg-sp}^2 and \mathbf{s}_{sp-sp}^2 are the signal-spontaneous and spontaneous-spontaneous beat terms, respectively. For photodetectors preceded by a lumped semiconductor optical amplifier, these terms are (see for example [10]):

$$\begin{aligned} \mathbf{s}_{sg}^2 &= 2 \cdot e \cdot R \cdot G \cdot P_{opt}, & \mathbf{s}_{sg-sp}^2 &= 4 \cdot R^2 \cdot S_{sp} \cdot G \cdot P_{opt}, \\ \mathbf{s}_{sp}^2 &= 4 \cdot e \cdot R \cdot S_{sp} \cdot \Delta n_{opt}, & \mathbf{s}_{sp-sp}^2 &= 4 \cdot R^2 \cdot S_{sp}^2 \cdot \Delta n_{opt}, \end{aligned} \quad (20)$$

where G is the amplifier gain, Δn_{opt} is the optical bandwidth, R is the detector efficiency and S_{sp} is the Amplified Spontaneous Emission (ASE) noise spectral density. R and S_{sp} are given by:

$$R = \frac{\hbar \cdot e}{\hbar \omega}, \quad S_{sp} = n_{sp} \cdot \hbar \omega \cdot (G - 1), \quad (21)$$

where \hbar is the detector quantum efficiency and n_{sp} is the population inversion coefficient. Now, for a distributed amplifier consisting of N sections, each one with gain G_n and population inversion coefficient $n_{sp,n}$, where n goes from 1 to N , we can write the total ASE spectral density as the sum of the spontaneous emission spectral density produced by each section, multiplied by the gain of the remaining sections after it, or:

$$S_{sp} = \sum_{n=1}^N n_{sp,n} \cdot \hbar \omega \cdot (G_n - 1) \cdot \prod_{m=n+1}^N G_m. \quad (22)$$

For the case where the population inversion factor is the same for all sections, we find that:

$$S_{sp} = n_{sp} \cdot \hbar \omega \cdot \sum_{n=1}^N (G_n - 1) \cdot \prod_{m=n+1}^N G_m = n_{sp} \cdot \hbar \omega \cdot (G_1 \cdot G_2 \cdot \dots \cdot G_N - 1) = n_{sp} \cdot \hbar \omega \cdot (G_T - 1), \quad (23)$$

where $G_T = G_1 \cdot G_2 \cdot \dots \cdot G_N$ is the total gain of the amplifier.

If we consider now a distributed amplifier, where both n_{sp} and the gain per unit length, g , depend on the position z along the device, we can transform the previous sum into an integral, taking into account that the spontaneous emission spectral density generated in a section of the device of length dz will be:

$$dS_{sp} = n_{sp}(z) \cdot \hbar \omega \cdot (e^{g(z) \cdot dz} - 1) = n_{sp}(z) \cdot \hbar \omega \cdot g(z) \cdot dz + o(dz^2). \quad (24)$$

The total ASE spectral density is then:

$$S_{sp} = \hbar \omega \cdot \int_0^L n_{sp}(z) \cdot g(z) \cdot e^{\int_z^L g(x) \cdot dx} \cdot dz. \quad (25)$$

For a device where both the population inversion coefficient and the gain per unit length are constant:

$$S_{sp} = n_{sp} \cdot \hbar \omega \cdot \int_0^L e^{g \cdot (L-z)} \cdot g \cdot dz = n_{sp} \cdot \hbar \omega \cdot (e^{g \cdot L} - 1) = n_{sp} \cdot \hbar \omega \cdot (G_T - 1), \quad (26)$$

where in this case $G_T = e^{g \cdot L}$ is the total device gain.

Therefore, both distributed models produce results that are consistent with classical lumped amplifier models, and they will be used in simulations for the noise characteristics of TAP detectors.

4.1. Parallel configuration

In parallel TAP detectors, amplification and absorption occur in a continuous way all along the device. In order to find the amount of absorbed ASE spectral density, we need therefore to perform a double integral along the device, once for absorption, and once for gain, as shown in Fig. 8 and expressed through the equation:

$$R \cdot S_{sp} = \frac{e}{\hbar \omega} \cdot \int_0^L \Gamma_{abs} \cdot \mathbf{a}_{abs} \cdot \left(\int_0^L n_{sp} \cdot \hbar \omega \cdot e^{\Delta g |x-z|} \cdot \Gamma_g \cdot g \cdot dz \right) \cdot dx, \quad (27)$$

which after integration yields:

$$R \cdot S_{sp} = 2 \cdot e \cdot n_{sp} \cdot \Gamma_{abs} \cdot \mathbf{a}_{abs} \cdot \Gamma_g \cdot g \cdot \frac{e^{\Delta g \cdot x} - (1 + \Delta g \cdot L)}{\Delta g^2} \approx e \cdot n_{sp} \cdot (\Gamma_{abs} \cdot \mathbf{a}_{abs} \cdot L) \cdot (\Gamma_g \cdot g \cdot L), \quad (28)$$

where the last approximation is valid when the net modal gain is small ($\Delta g \cdot L \ll 1$). This is an interesting result, since it expresses that the absorbed ASE spectral density is proportional to the square of the TAP detector length, due to the fact that both amplification and absorption occur all along the device. Note that the integral is defined so that ASE propagating in the opposite direction as the input optical signal is also accounted for.

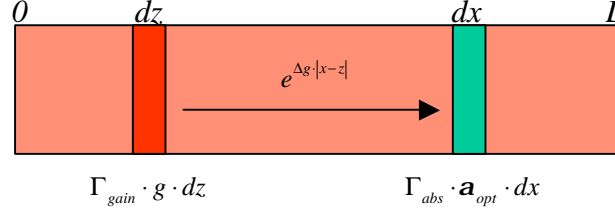


Fig. 8: Distributed noise model for parallel TAP detectors. The quantities indicated are the amount of spontaneous emission generated at z , the amplification that it suffers from z to x , and the fraction of it absorbed at x .

4.2. Sequential configuration

Applying to the sequential configuration the discrete model described above, assuming that all amplifier sections have the same gain and population inversion factor, G_2 and $n_{sp,2}$, except for the first one, for which we assume G_1 and $n_{sp,1}$, we find that the absorbed spontaneous emission spectral density is given by:

$$R \cdot S_{sp} = e \cdot \mathbf{h}_{det} \cdot \left[n_{sp,1} \cdot (G_1 - 1) \cdot \sum_{n=1}^N \Delta G^{n-1} + n_{sp,2} \cdot (G_2 - 1) \cdot \sum_{n=2}^N \left(\sum_{m=1}^{n-1} \Delta G^{n-m-1} + \sum_{l=n}^N \Delta G^{l-n} \right) \right], \quad (29)$$

where we have assumed that the ASE generated in each gain section is absorbed in every detection section, both forward and backward with respect to the input optical signal propagation direction. The effect of net gain per period in the propagating ASE has also been accounted for. We can finally find:

$$R \cdot S_{sp} = e \cdot \mathbf{h}_{det} \cdot \left[n_{sp,1} \cdot (G_1 - 1) \cdot \frac{\Delta G^N - 1}{\Delta G - 1} + 2 \cdot n_{sp,2} \cdot (G_2 - 1) \cdot \frac{\Delta G^N - (1 + N \cdot (\Delta G - 1))}{(\Delta G - 1)^2} \right] \approx N \cdot e \cdot \mathbf{h}_{det} \cdot \left[n_{sp,1} \cdot (G_1 - 1) + n_{sp,2} \cdot (G_2 - 1) \cdot (N - 1) \right], \quad (30)$$

where the approximation is valid when $\Delta G \approx 1$. This is an interesting result, since it shows that, both population inversion factors being in the same order of magnitude, the noise in sequential TAP detectors is very similar to the one in photodetectors preceded by SOAs when $(G_1 - 1) \gg (G_2 - 1) \cdot (N - 1)$, which is possible, since G_1 can be made large, while G_2 can be small, since it's only needed to compensate for the absorbed power in the detection sections and the losses.

4.3. Noise Figure

As always, we define the output and input Signal-to-Noise Ratio of a photodetector, SNR_{out} and SNR_{in} respectively, and its Noise Figure NF as:

$$SNR_{out} = \frac{|I|^2}{\langle i_N^2 \rangle}, \quad SNR_{in} = \frac{P_{opt}}{2 \cdot \hbar \omega \cdot \Delta f}, \quad NF = \frac{SNR_{in}}{SNR_{out}}, \quad (31)$$

where I denotes the photocurrent. The Noise Figure is a very important parameter in optical communications, since it measures the amount of noise added by a device to the transmitted signal. In order to calculate it, we can insert the equations (28) and (30) into (19) and (20), and use (31), as well as make the substitution $I = R \cdot G \cdot P_{opt}$, since this term in the classical lumped amplifier model represents the amount of photocurrent generated by the absorption of the amplified input signal. Fig. 9 shows the Noise Figure for both sequential and parallel TAP detectors, comparing them to those of traditional TAPDs, with and without an optical preamplifier, respectively.

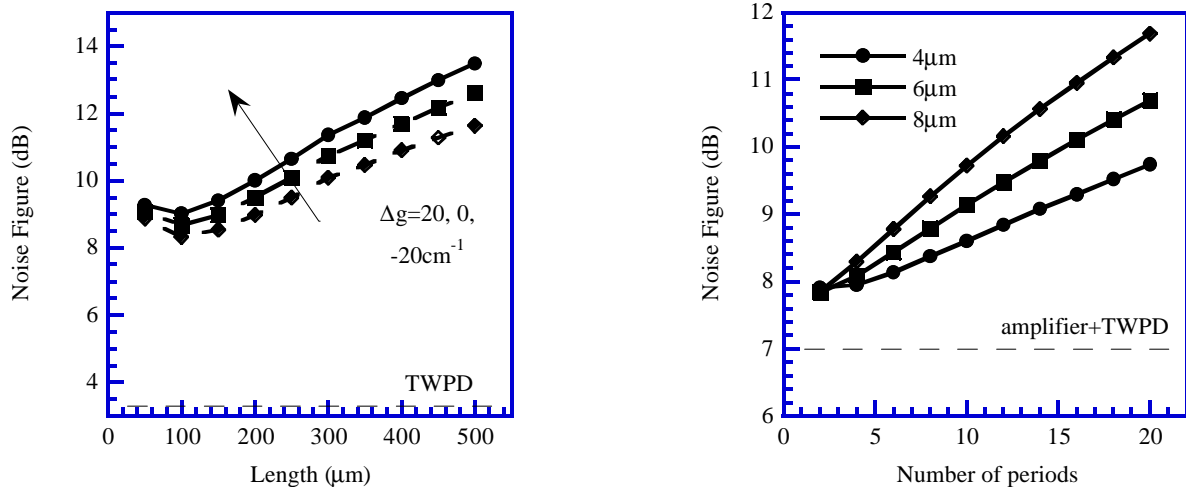


Fig. 9: Noise Figure for parallel (left) and sequential (right) TAP detectors, compared to the noise figures of traditional TAPDs without and with optical preamplification respectively.

For parallel TAP detectors, we have plotted the Noise Figure for different values of the net modal gain, showing that for increasing Δg , the noise penalty decreases, being ~ 6 dB for devices between 100 and 200 μm . The optimum length for parallel TAP detectors is then between 150 and 200 μm , where the bandwidth-efficiency product has reached its steady value, and the noise penalty is still minimum. We can see that there is a net increase in the dynamic range of ~ 7 dB with respect to traditional TAPDs, since there was an increase of ~ 13 dB in the saturation power.

For sequential TAP detectors, plots with different net gain per period have been omitted, since the change in the Noise Factor is smaller than 0.2 dB when ΔG goes from 0.94 to 1.06. In the graph we can observe that there is an increase of ~ 2 dB in the Noise Factor for devices with 10 periods, with respect to TAPDs preceded by a single optical amplifier. This is then the optimum number of device periods, since it presents lowest noise penalty of all the ones that exhibit highest bandwidth-efficiency product when there is no net gain per period. We can also observe that, since there was an increase of ~ 5 dB in saturation power, sequential TAP detectors exhibit a dynamic range ~ 3 dB larger than traditional photodetectors with preamplification.

5. CONCLUSION

We have developed simulation models to analyze the performance of TAP detectors, both in their sequential and parallel configurations. Based on traditional distributed element models, and either modifying them or combining them with an ABCD matrix technique, we have calculated the microwave performance of TAP detectors. In the case of the parallel configuration, theoretical and experimental results show very good agreement, validating our model. Using a distributed photocurrent model, we have found the efficiency and bandwidth of TAP detectors. Finally, a distributed noise model was developed and used to find the noise penalty introduced by these devices. The results from these simulations, when compared to other photodetectors with similar bandwidth-efficiency products, yield a net increase in the dynamic range, which we were able to quantify.

REFERENCES

- [1] K.S. Giboney, R.L. Nagarajan, T.E. Reynolds, S.T. Allen, R.P. Mirin, M.J.W. Rodwell and J.E. Bowers, "Traveling-wave photodetectors with 172-GHz bandwidth and 76-GHz bandwidth-efficiency product", *Photonics Tech. Lett.*, vol. 7, no. 4, Apr. 1995, pp. 412-14.
- [2] D. Wake, "A 1550-nm millimeter-wave photodetector with a bandwidth-efficiency product of 2.4 THz", *J. Lightwave Tech.*, vol. 10, no. 7, July 1992, pp. 908-12.

- [3] L.Y. Lin, M.C. Wu, T. Itoh, T.A. Vang, R.E. Muller, D.L. Sivco and A.Y. Cho, "Velocity-matched distributed photodetectors with high saturation power and large bandwidth", *IEEE Photonics Tech. Lett.*, vol. 8, no. 10, Oct. 1996, pp. 1376-8.
- [4] D. Lasoosa Y.J. Chiu, J. Piprek and J.E. Bowers, "Traveling-wave amplification photodetector (TAP detector)", *Proc. IEEE LEOS 13th Annual Meeting*, vol. 1, Rio Grande, Puerto Rico: Lasers and Electro-Optics Society, Nov. 2000, pp. 260-1.
- [5] H. Hasegawa and H. Okizaki, "M.I.S. and Schottky slow-wave coplanar striplines on GaAs substrates", *Electron. Lett.*, vol. 13, no. 22, Oct. 1977, pp. 663-4.
- [6] K.S. Giboney, M.J.W. Rodwell and J.E. Bowers, "Traveling-wave photodetector theory", *IEEE Trans. Microw. Theory Tech.*, vol. 45, no. 8, pt. 2, Aug. 1997, pp. 1310-19.
- [7] G. Gonzalez, "Microwave transistor amplifiers, analysis and design", 2nd Ed., Upper Saddle River, NJ: Prentice Hall, 1997.
- [8] R.E. Collin, "Foundations for microwave engineering", 2nd Ed., New York: McGraw-Hill, 1992.
- [9] K.S. Giboney, M.J.W. Rodwell and J.E. Bowers, "Traveling-wave photodetector design and measurements", *IEEE J. Selected Topics in Quantum Electr.*, vol. 2, no. 3, Sep. 1996, pp. 622-9.
- [10] G.P. Agrawal, "Fiber-optic communication systems", 2nd Ed., New York: Wiley and Sons, 1992.